Monthly Notices
of the
ROYAL ASTRONOMICAL SOCIETY

MNRAS **449,** 629–638 (2015) doi:10.1093/mnras/stv306

Evolution of binary stars in multiple-population globular clusters

Jongsuk Hong,[1]⋆ Enrico Vesperini,[1] Antonio Sollima,[2] Stephen L. W. McMillan,[3] Franca D'Antona[4] and Annibale D'Ercole[2]

[1]*Department of Astronomy, Indiana University, Bloomington, IN 47401, USA*
[2]*INAF – Osservatorio Astronomico di Bologna, via Ranzani 1, I-40127 Bologna, Italy*
[3]*Department of Physics, Drexel University, Philadelphia, PA 19104, USA*
[4]*INAF – Osservatorio Astronomico di Roma, via di Frascati 33, I-00040 Monteporzio, Italy*

Accepted 2015 February 10. Received 2015 February 4; in original form 2014 November 24

ABSTRACT

The discovery of multiple stellar populations in globular clusters has implications for all the aspects of the study of these stellar systems. In this paper, by means of *N*-body simulations, we study the evolution of binary stars in multiple-population clusters and explore the implications of the initial differences in the spatial distribution of different stellar populations for the evolution and survival of their binary stars. Our simulations show that initial differences between the spatial distribution of first-generation (FG) and second-generation (SG) stars can leave a fingerprint in the current properties of the binary population. SG binaries are disrupted more efficiently than those of the FG population resulting in a global SG binary fraction smaller than that of the FG. As for surviving binaries, dynamical evolution produces a difference between the SG and the FG binary binding energy distribution with the SG population characterized by a larger fraction of high binding energy (more bound) binaries. We have also studied the dependence of the binary properties on the distance from the cluster centre. Although the global binary fraction decreases more rapidly for the SG population, the local binary fraction measured in the cluster inner regions may still be dominated by SG binaries. The extent of the differences between the surviving FG and SG binary binding energy distribution also varies radially within the cluster and is larger in the cluster inner regions.

Key words: stars: chemically peculiar – globular clusters: general.

1 INTRODUCTION

Numerous observational studies have revealed that globular clusters host multiple stellar populations characterized by different chemical (see e.g. Carretta et al. 2009a,b; Gratton, Carretta & Bragaglia 2012, and references therein) and photometric properties (see e.g. Lee et al. 1999; Bedin et al. 2004; Ferraro et al. 2004; Piotto et al. 2007, 2015; Milone et al. 2008, 2010, 2012; Bellini et al. 2013). The implications of the presence of multiple populations in globular clusters and the questions raised by this discovery span all the aspects of the astrophysics of these stellar systems including their formation, chemical and dynamical evolution along with the possible role played by these objects in the assembly of the Galactic halo.

A complete scenario for the formation and evolution of multiple-population globular clusters requires the identification of the source(s) of gas with chemical properties consistent with the observed abundance patterns and out of which second-generation (SG) stars might have formed along with models following the dynamics of this gas, the SG formation history and the subsequent early- and long-term dynamical evolution of the multiple-population cluster. Different sources of gas for the SG formation have been suggested in the literature (see e.g. Ventura et al. 2001; Prantzos & Charbonnel 2006; Decressin et al. 2007, de Mink et al. 2009; Bastian et al. 2013) and a number of studies have addressed some of the issues concerning the origin of the observed abundance patterns (see e.g. Decressin et al. 2007, D'Ercole et al. 2008, 2010, 2012), the formation and dynamical evolution of multiple-population clusters (see e.g. D'Ercole et al. 2008; Decressin, Baumgardt & Kroupa 2008; Decressin et al. 2010; Vesperini et al. 2010, 2013; Bekki 2011). The theoretical study of multiple-population clusters is still in its infancy and most questions and challenges are just now beginning to be addressed.

In D'Ercole et al. (2008), we have modelled the formation and dynamical evolution of the SG population forming from the ejecta of first-generation (FG) intermediate-mass Asymptotic Giant Branch (AGB) stars; one of the predictions of our study was that the SG population would form in a compact subsystem concentrated in the inner regions of the FG cluster. In a

⋆ E-mail: hongjong@indiana.edu

subsequent study on the long-term evolution of multiple-population clusters (Vesperini et al. 2013), we have shown that some memory of the initial spatial segregation of the SG population should be preserved in many Galactic clusters and, indeed, several observational studies (see e.g. Sollima et al. 2007; Bellini et al. 2009; Lardo et al. 2011; Milone et al. 2012; Beccari et al. 2013; Johnson & Pilachowski 2012; Cordero et al. 2014; Kucinskas, Dobrovolskas & Bonifacio 2014) have found clusters in which SG stars are more spatially concentrated than FG stars (see also Bellazzini et al. 2012; Richer et al. 2013, for interesting studies on the kinematical properties of FG and SG stars).

One of the dynamical implications of the SG spatial segregation concerns the evolution of binary stars. Until SG and FG stars are completely mixed, SG stars will evolve in a denser environment where disruption and evolution of SG binaries will occur more rapidly than for FG binaries. In Vesperini et al. (2011), we have carried out an initial investigation of this issue by combining *N*-body and semi-analytical calculations of the disruption of binaries in multiple-population clusters. Our study showed that SG binary disruption rate can indeed be significantly larger than that of FG binaries and that the overall binary disruption rate in multiple-population clusters is larger than that of a single-population (SP) cluster without the central SG dense subsystem.

An early investigation by D'Orazi et al. (2010), although based on a small sample of Ba stars, suggests that the fraction of SG binaries might indeed be smaller than that of FG binaries.

As for the connection with observational studies, as already pointed out in Vesperini et al. (2011) and further discussed in more detail in this paper, it is important to emphasize the differences between the theoretical predictions concerning the global binary fraction and the local binary fraction measured at different distances from the cluster centre. Specifically, we will show in this paper that even if the global SG binary fraction is smaller than the FG one, the local SG binary fraction measured in the cluster innermost regions may still be larger than the FG one.

In this paper, we extend the initial investigation by Vesperini et al. (2011) by carrying out a survey of *N*-body simulations and including in a self-consistent way a population of binary stars instead of just relying on analytical estimates for binary disruption rates due to single/binary interactions. The *N*-body simulations presented here, while still idealized in several aspects, allow us to follow in much more detail the evolution of the cluster binary population and its dynamics. The questions we address in this paper concern the radial variation of the fraction of FG and SG binary stars resulting from the combined effect of disruption and tendency of binary stars to segregate in the cluster inner regions, the evolution of the global binary fraction and its relation with the local fraction measured at different distances from the cluster centre, and the evolution of the binding energy of the surviving binaries.

The results of our investigation show that differences in the initial structural properties of the FG and SG populations can leave a significant fingerprint in the properties of FG and SG binaries.

The outline of this paper is the following. In Section 2, we describe the method and the initial conditions adopted in our simulations. In Section 3 we present our results, and in Section 4 we summarize the main conclusions of our investigation.

2 METHODS AND INITIAL CONDITIONS

The *N*-body simulations presented in this paper have been carried out with the GPU-accelerated version of the code NBODY6 (Aarseth 2003; Nitadori & Aarseth 2012) and run on the BIG RED II cluster at Indiana University.

In the initial conditions we have explored, the FG and SG subsystems have initially the same total mass and they both follow a King model (1966) density profile with central dimensionless potential $W_0 = 7$; the SG subsystem, however, is initially concentrated in the inner regions of the FG system as suggested by the results of D'Ercole et al. (2008). All the simulations start with equal-mass particles. We have explored two models here: one in which the initial ratio of the FG to SG half-mass radius ($R_{\rm h,\,FG}/R_{\rm h,\,SG}$) is equal to 5, and one with $R_{\rm h,\,FG}/R_{\rm h,\,SG} = 10$. In order to explore the differences between SP and multiple-population clusters we have also run a number of simulations of SP systems with the same number of particles and tidal radius as the multiple-population systems but with an internal structure described by a single King model with $W_0 = 7$.

We include the effects of the host galaxy tidal field (modelled as a point mass) and assume that the cluster is initially tidally truncated; particles moving beyond a radius equal to two times the tidal radius are removed from the simulation.

As far as the properties of the binary population are concerned, we have explored the evolution of systems with values of the initial binary fraction, $f_{\rm b,\,0} = N_{\rm bin}/(N_{\rm s} + N_{\rm bin})$ equal to 0.03 and 0.10 (where $N_{\rm s}$ is the number of single particles and $N_{\rm bin}$ is the number of binaries; we will refer to $N = N_{\rm bin} + N_{\rm s}$ to indicate the sum of the total number of single and binary particles; the total number of particles in each simulation is equal to $N_{\rm tot} = N_{\rm s} + 2N_{\rm bin}$). All the simulations start with $N = 20\,000$ ($N_{\rm tot} = 22\,000$ for simulations with $f_{\rm b,\,0} = 0.1$, and $N_{\rm tot} = 20\,600$ for simulations with $f_{\rm b,\,0} = 0.03$). We assume that FG and SG binaries have the same initial binding energy distribution. In this paper, we focus our attention on moderately hard binaries with initial global hardness parameter, $x_{\rm g,\,0}$, ranging from 3 to 20; $x_{\rm g,\,0}$ is defined as $E_{\rm b}/(m\sigma^2_{\rm SP})$ where $E_{\rm b}$ is the absolute value of the binary binding energy, and $\sigma_{\rm SP}$ the 1D velocity dispersion of all stars in the SP system. In order to better illustrate the dependence of the binary evolution on the hardness parameter, we have run a number of simulations each one including binaries with a single value of $x_{\rm g,\,0}$. We have also carried out one simulation including binaries with a uniform binding energy distribution between $x_{\rm g,\,0} = 3$ and 20.

The initial parameters of all models and the ids used to identify them in the rest of this paper are summarized in Table 1. Some of the simulations performed reach a deep core collapse phase; specifically the following systems reach the deep core collapse phase (MPr5f03x3, MPr5f03x5, MPr10f1x3, MPr10f1x5, MPr10f1x10, MPr10f1x20, MPr5f1x3, MPr5f1x5, SPf1x3) at $t/\tau_{\rm rh,\,0}$ equal to about, respectively, (8.4, 8.7, 4.9, 4.9, 5.7, 7.8, 7.3, 8.3, 15.5).

In order to provide an indication of the extent of the stochastic variations in the results obtained we have carried out 10 simulations with different random realizations of the initial conditions for the system MPr5f03x5 and 10 for the system MPr5f03x20. Three simulations with $N = 32\,000$, 40 000 and 60 000 and structural properties equal to those of MPr5f03x10 have also been carried out to explore the dependence of the results on the number of particles.

3 RESULTS

3.1 Evolution of the global binary fraction

Fig. 1 shows the time evolution of the global binary fraction for the multiple-population systems MPr5f1x3, MPr5f1x5, MPr5f1x10, MPr5f1x20, MPr5f1x3-20, and the corresponding SP systems

Table 1. Initial parameters for all models. $N = N_s + N_{bin}$ is the total number of single, N_s, and binary, N_{bin}, particles. $f_{b,0} = N_{bin}/(N_s + N_{bin})$ is the initial binary fraction. $\frac{R_{h,FG}}{R_{h,SG}}$ is the ratio of the FG to the SG initial half-mass radii. All the SP models refer to single-population systems. $x_{g,0}$ is the initial hardness parameter (see Section 2 for definition).

Model id.	N	$\frac{R_{h,FG}}{R_{h,SG}}$	$f_{b,0}$	$x_{g,0}$
MPr5f03x3	20 000	5	0.03	3
MPr5f03x5	20 000	5	0.03	5
MPr5f03x10	20 000	5	0.03	10
MPr5f03x20	20 000	5	0.03	20
MPr10f03x3	20 000	10	0.03	3
MPr10f03x5	20 000	10	0.03	5
MPr10f03x10	20 000	10	0.03	10
MPr10f03x20	20 000	10	0.03	20
MPr5f1x3	20 000	5	0.1	3
MPr5f1x5	20 000	5	0.1	5
MPr5f1x10	20 000	5	0.1	10
MPr5f1x20	20 000	5	0.1	20
MPr5f1x3-20	20 000	5	0.1	3–20[a]
SPf1x3	20 000	–	0.1	3
SPf1x5	20 000	–	0.1	5
SPf1x10	20 000	–	0.1	10
SPf1x20	20 000	–	0.1	20
SPf1x3-20	20 000	–	0.1	3–20[a]
MPr5f03x10n32k	32 000	5	0.03	10
MPr5f03x10n40k	40 000	5	0.03	10
MPr5f03x10n60k	60 000	5	0.03	10

Note. [a]A uniform distribution in binding energy is assumed.

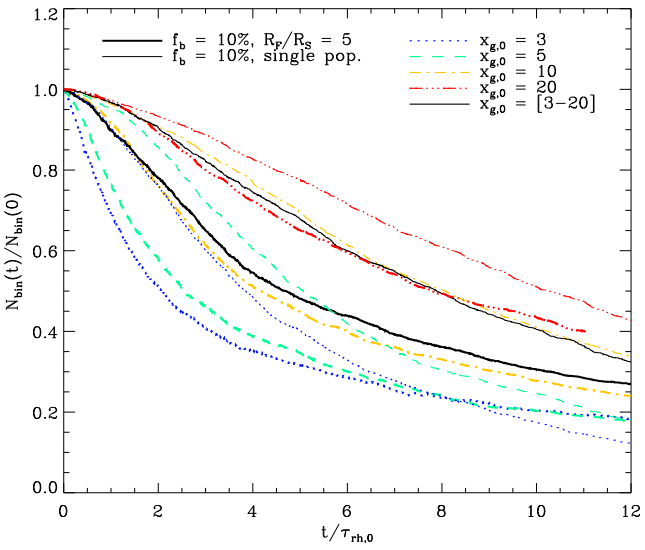

Figure 1. Time evolution of the total number of binaries, $N_{bin}(t)$ (normalized to the total initial number of binaries, $N_{bin}(0)$), for simulations MPr5f1 and SPf1 and different values of the hardness factor $x_{g,0}$. Time is normalized to the initial half-mass relaxation time, $\tau_{rh,0}$.

SPf1x3, SPf1x5, SPf1x10, SPf1x20, SPf1x3-20. As shown by this figure, multiple-population systems are characterized by a general enhancement in the binary disruption compared to SP clusters. As discussed in Vesperini et al. (2011), the differences in the structural properties between multiple-population and SP clusters are responsible for the observed differences in the evolution of the global binary fraction.

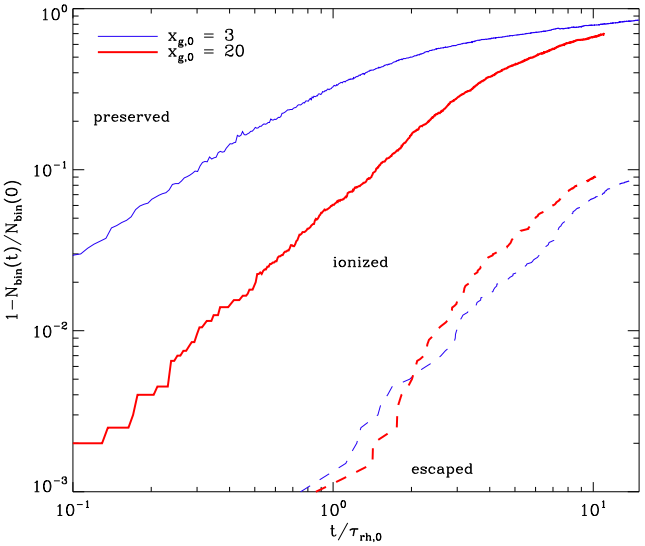

Figure 2. Time evolution (with time normalized to the initial half-mass relaxation time) of the total number of binaries (normalized to the total initial number of binaries). At any given time the difference between 1 and the value shown by the solid line represents the fraction of the initial binary population surviving in the cluster, the difference between the values shown by the solid line and the dashed line represents the fraction of the initial number of binaries ionized, and the dashed line shows the fraction of the initial number of binaries escaped from the cluster. Thick, red lines refer to the MPr5f1x20 simulation; thin blue lines refer to the MPr5f1x3 simulation.

The role of different processes responsible for the decrease in the number of binaries is illustrated in Fig. 2 for the simulations MPr5f1x3 and MPr5f1x20. For the range of binding energies considered in this paper, binary ionization is the dominant process while binary escape plays only a minor role. Ionization is more efficient in the central high-density regions populated mainly by SG binaries and, as we will further discuss below, this leads to a significant preferential disruption of SG binaries. As expected, simulations with binaries with smaller values of $x_{g,0}$ are characterized by a more rapid ionization of a larger fraction of binaries.

Binary escape affects primarily FG binaries but the preferential escape of FG binaries is far from being sufficient to balance the preferential ionization of SG binaries with the net result that the global fraction of SG binaries declines much more rapidly. Fig. 3 show the number of FG, SG and mixed binaries (hereafter we refer to binaries that, as a result of a component exchange event, have one SG and one FG component as mixed binaries) escaping for the MPr5f1x3 and the MPr5f1x20 simulations. This figure further illustrates the role of escape in determining the decrease of the global binary fraction and shows the extent to which SG, FG and mixed binaries are affected by this process.

In Fig. 4 we show the time evolution of total number of SG and FG and mixed binaries. This figure clearly illustrates the preferential disruption of SG binaries in all the systems considered in this paper; it is also interesting to note that exchange events, particularly for simulations with the harder binaries, lead to the formation of a non-negligible number of mixed binaries.

A comparison of the panels of Fig. 4 showing the results for the MPr5 and the MPr10 simulations, show that, as was to be expected, systems starting with a more concentrated SG subsystem are characterized by a more efficient disruption of SG binaries. Even

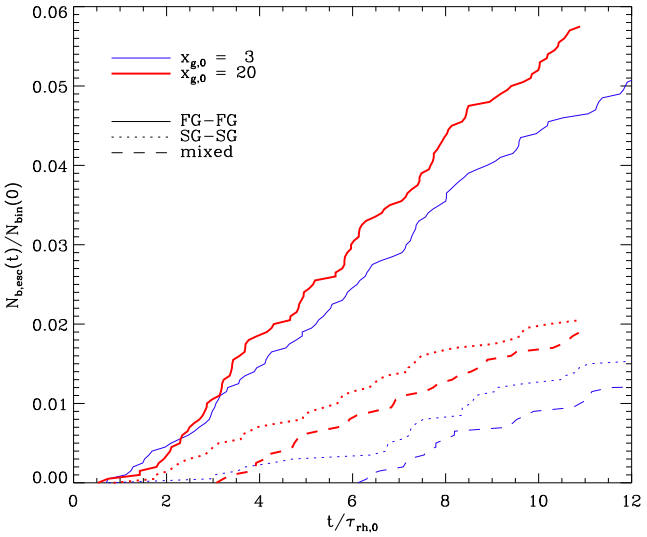

Figure 3. Time evolution (time is normalized to the initial half-mass relaxation time) of the total number of escaping binaries (normalized to the total initial number of binaries, $N_{\rm bin}(0)$). Thick, red lines refer to the MPr5f1x20 simulation; thin blue lines refer to the MPr5f1x3 simulation. Solid, dotted and dashed lines refer, respectively, to FG, SG and mixed binaries.

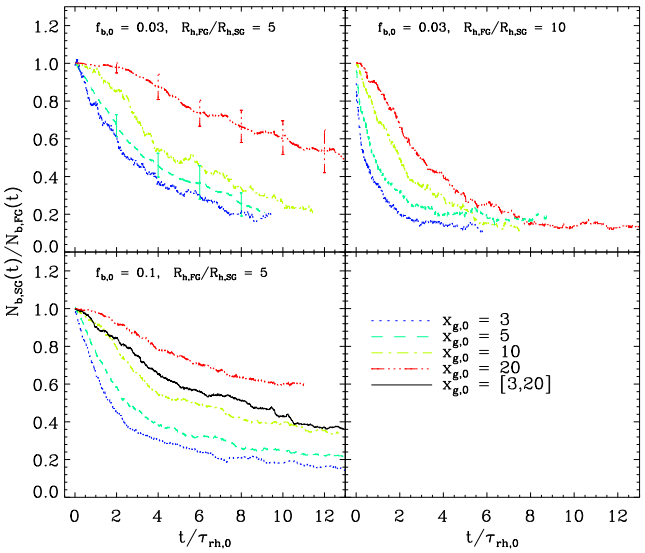

Figure 5. Time evolution (with time normalized to the initial half-mass relaxation time) of the SG-to-FG binary number ratio for MPr5f03 (upper-left panel), MPr10f03 (upper-right panel) and MPr5f1 (lower-left panel) for different values of $x_{g,0}$ (see lower-right panel for colours and line styles corresponding to the different values of $x_{g,0}$). For simulations MPr5f03x5 and MPr5f03x20 in the upper-left panel, the lines show the mean of the SG-to-FG binary number ratio from the results of the 10 simulations with different random realizations of the initial conditions; bars showing the $\pm 1\sigma$ are also shown at a few representative times.

for the $x_{g,0} = 20$ case, only about 6 per cent of the initial population of SG binaries survive after about $10\tau_{rh,0}$ in the MPr10f03x20 simulation whereas in the less concentrated MPr5f03x20 system about 15 per cent of the initial SG binary population survives after the same number of initial half-mass relaxation times. Fig. 5 shows the time evolution of the ratio of the total number of SG to the total number of FG binaries and further illustrates the preferential disruption of SG binaries. For the simulations MPr5f03x5 and MPr5f03x20, the plots in Figs 4 and 5 show, respectively, the mean values of the number of binaries and the mean of the SG-to-FG binary number ratio along with the 1σ variation about the mean as

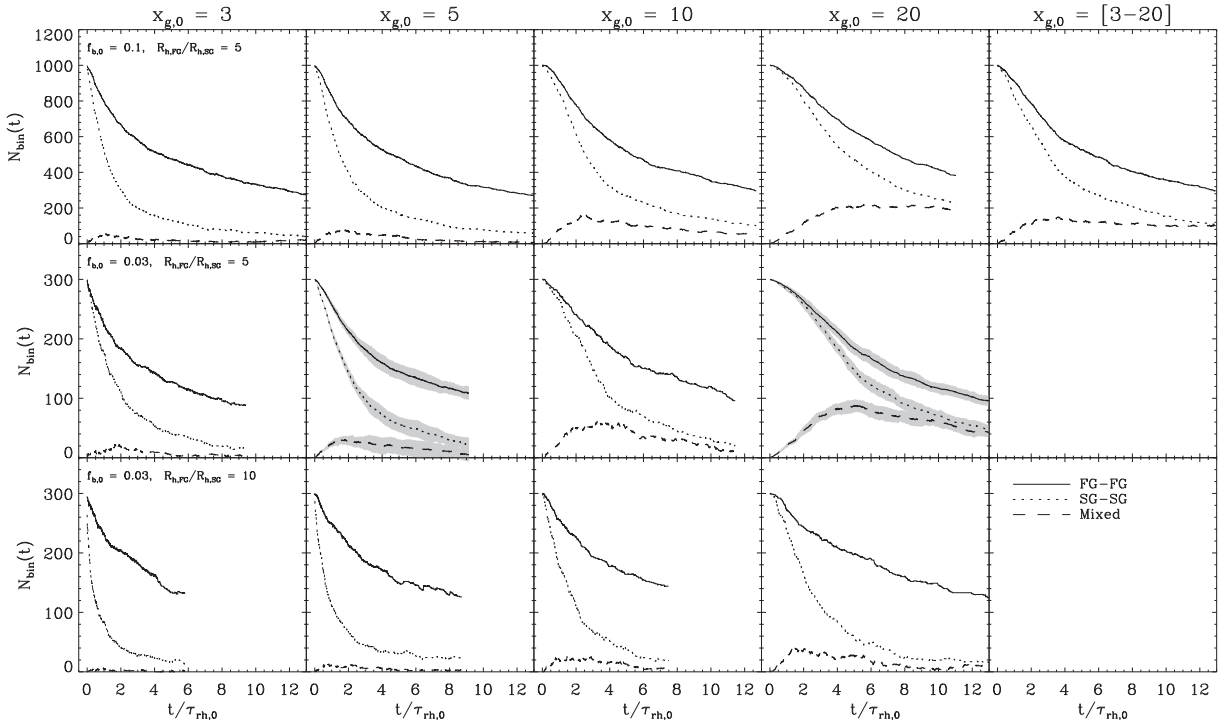

Figure 4. Time evolution of the total number of FG (solid lines), SG (dotted lines) and mixed (dashed lines) binaries for all the MPr5f1 (first row), MPr5f03 (second row) and MPr10f03 (third row) simulations. Each column shows the results of simulations for a different value of $x_{g,0}$ indicated at the top of the figure. For simulations MPr5f03x5 and MPr5f03x20 the lines show the mean of the number of binaries from the results of the 10 simulations with different random realizations of the initial conditions and the shaded area show the $\pm 1\sigma$. Time is normalized to the initial half-mass relaxation time.

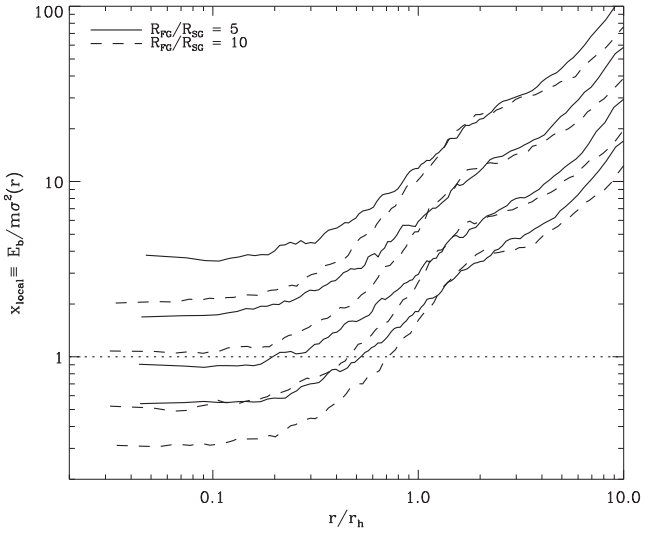

Figure 6. Radial profiles of initial local hardness parameter, $x_{\rm local}(r)$ (see Section 3.1 for definition) for the MPr5f03 (solid lines) and the MPr10f03 (dashed lines) simulations. Different solid (and dashed) lines correspond (from top to bottom) to $x_{\rm g,\,0} = 20$, 10, 5, 3. Radius is normalized to the half-mass radius, $r_{\rm h}$.

calculated from ten different realizations of each of these two initial conditions.

In Fig. 6 we show the radial profile of the local hardness parameter $x_{\rm local}(r)$, defined as the ratio of the binary binding energy to $m\sigma(r)^2$ where $\sigma(r)$ is the 1D velocity dispersion measured at a distance r from the cluster centre. This parameter provides a more specific measure of binary hardness and of the expected dynamical fate of a binary as a function of the distance from the cluster centre. SG binaries are concentrated in the cluster inner regions where the larger velocity dispersion results in smaller values of $x_{\rm local}(r)$ and a more rapid disruption.

For binaries in the cluster outer regions (preferentially FG binaries), on the other hand, $x_{\rm local}$ is large and binaries can easily survive. FG binaries initially orbiting in the cluster outer regions can be disrupted only later in the cluster evolution after migrating towards the cluster central regions as a result of the mass segregation process.

Figs 7 and 8 show the density of FG, SG and mixed binary stars in the r–$x_{\rm local}(r)$ and the r–$E_{\rm b}$ planes for the simulation MPr5f1x3-20. This figure illustrates the interplay between segregation and binary evolution. As binaries segregate towards the inner regions they are disrupted as a result of encounters with single stars or other binaries. Harder binaries, however, can survive and evolve to become harder. SG binaries are those more affected by these evolutionary processes (ionization and hardening) as clearly shown also by the histograms of $x_{\rm local}(r)$ and $E_{\rm b}$ in Figs 7 and 8. Figs 7 and 8 also show that while segregation leads to a decrease in the number of binaries in the cluster outer regions ($r > r_{\rm h}$, where $r_{\rm h}$ is the cluster half-mass radius), the distribution of binding energy of outer binaries is not evolving significantly. The effects of disruption and hardening are instead clearly visible in the distribution of binding energy of inner($r < r_{\rm h}$) binaries.

Finally, in Fig. 9, we show the time evolution of the total number of FG and SG binaries for simulations with different initial number of particles (MPr5f03x10n32k, MPr5f03x10n40k, MPr5f03x10n60k). Overall the results of our simulations show a small spread for systems with different number of particles. Since one of the mechanisms responsible for the decrease of the number of binaries is evaporation (although, as discussed above, it is not the dominant one), some spread is to be expected since the dependence of the evaporation time-scale on the number of particles differs from that of the relaxation time (see e.g. Fukushige & Heggie 2000; Baumgardt 2001).

3.2 Radial variation of the binary fraction

In this section, we focus our attention on the radial profiles of the FG and SG binary fraction. As anticipated in the initial discussion in Section 1, the predictions concerning the different evolution of the global fraction of FG and SG binaries and the general preferential disruption of SG binaries do not necessarily imply that the local binary fraction measured at different distances from the cluster centre follows the same trend.

In general, the details of the evolution of the radial variation of the SG-to-FG number ratio are determined by the complex interplay among binary ionization, hardening, rate of segregation and by differences in the initial spatial distribution of the FG and SG populations.

While, as shown in the previous section, the overall fraction of SG binaries decreases more rapidly than that of the FG population, locally the binary population can be dominated by SG binaries.

Fig. 10 shows the time evolution of the radial profile of the binary fraction for all the binaries (upper panel), for FG binaries (middle panel) and for SG binaries (lower panel) for the simulation MPr5f1x3-20. This figure illustrates the effect of segregation and binary disruption: segregation towards the cluster inner regions initially leads to an enhancement of the central binary fraction, binary disruption offsets the effects of segregation and causes the binary fraction in the central regions to decrease.

Fig. 11 shows the cumulative (upper panels) and the differential (lower panels) radial profiles of the SG-to-FG binary number ratio for the simulations MPr5f1x5, MPr5f1x20 and MPr5f1x3-20. We point out that although the global FG binary fraction is larger than the global SG binary fraction (see Fig. 4), in the inner regions the binary population can still be dominated by SG binaries while in the outer regions, the binary population is dominated by FG binaries.

Although our simulations are still focused on simplified models and not aimed at a direct comparison with observational data, it is important to emphasize the difference between the global SG and FG binary fractions and the local values of these fractions measured at different distances from the cluster centre. Observational studies focusing on the binary fraction in a limited range of radial distances from the cluster centre might reveal a larger fraction of FG or SG binaries depending on the radial position of the region probed by observations. The interpretation of observational results in the context of the preferential disruption of SG binaries described in this paper must therefore take into account the radial variation of the SG and FG binary fractions and the differences between local and global binary fraction of the two populations.

While more realistic simulations are needed for a close comparison with observational studies, we have further addressed this issue here and explored the time evolution of the distance, $R_{\rm glob}$, from the cluster centre where the local FG-to-SG binary number ratio equals the global value of this ratio. Fig. 12 shows the time evolution of $R_{\rm glob}$ for all the simulations presented in this paper. $R_{\rm glob}$ does not vary significantly during the cluster evolution and it does not significantly depend on the SG initial concentration or the binary fraction. $R_{\rm glob}$ lies between approximately $r_{\rm h}$ (for simulations with high-binding energy binaries, $x_{\rm g,\,0} \geq 5$) and 2–2.5$r_{\rm h}$

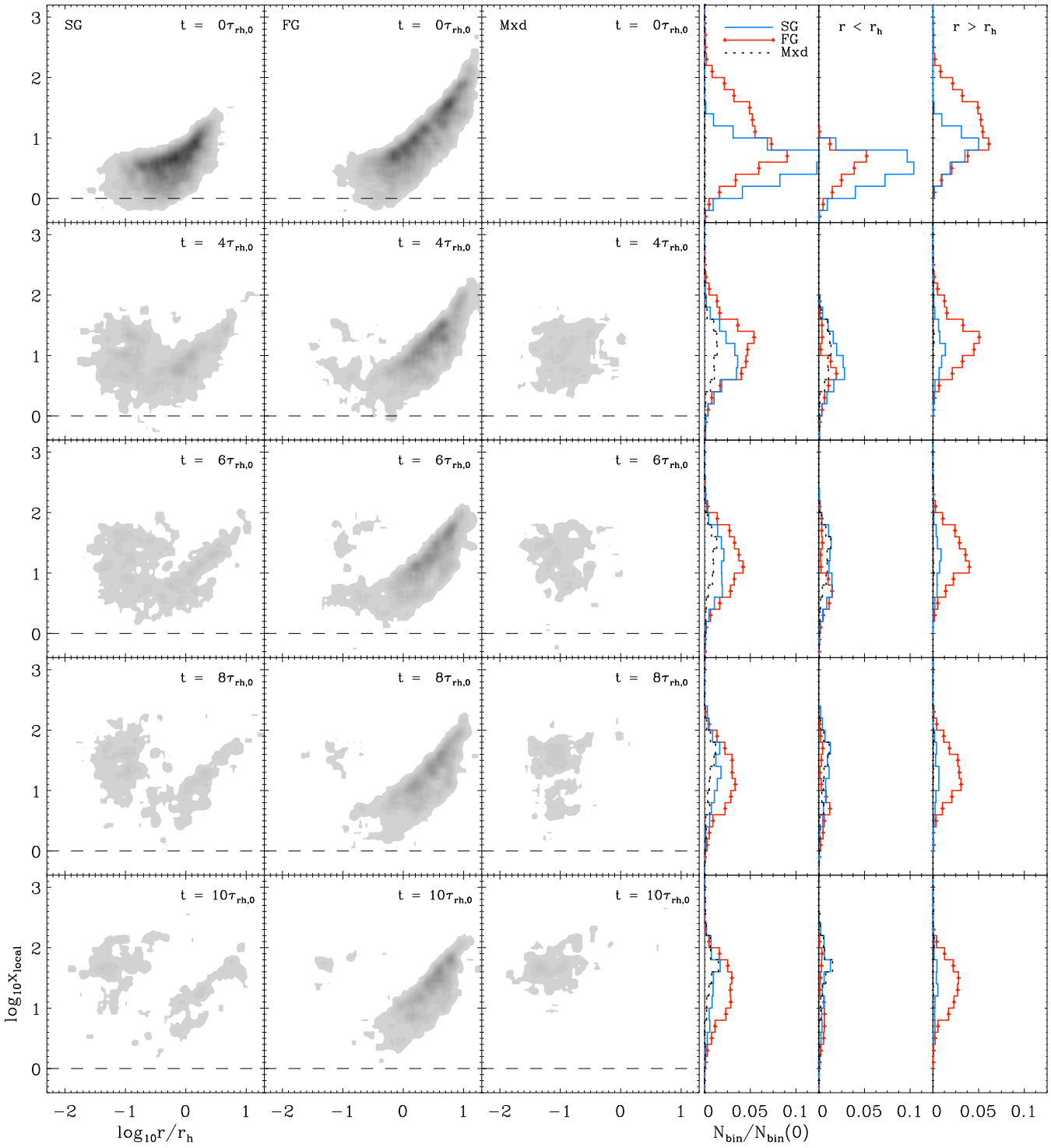

Figure 7. Time evolution of the density of SG (first column), FG (second column) and mixed (third column) binaries in the $\log(r/r_{\rm h})$–$\log(x_{\rm local}(r))$ plane (where $x_{\rm local}(r)$ is the local hardness parameter; see Section 3.1 for definition) for the MPr5f1x3-20 simulation. The last three columns of panels (on the right-hand side of the figure) show the histograms of the distribution of $\log(x_{\rm local}(r))$ for SG (solid blue lines), FG (red lines and short vertical segments) and mixed binaries (dashed lines) for the whole system, for binaries within the half-mass radius and outside the half-mass radius. Data from three combined snapshots around the indicated time are used for these plots.

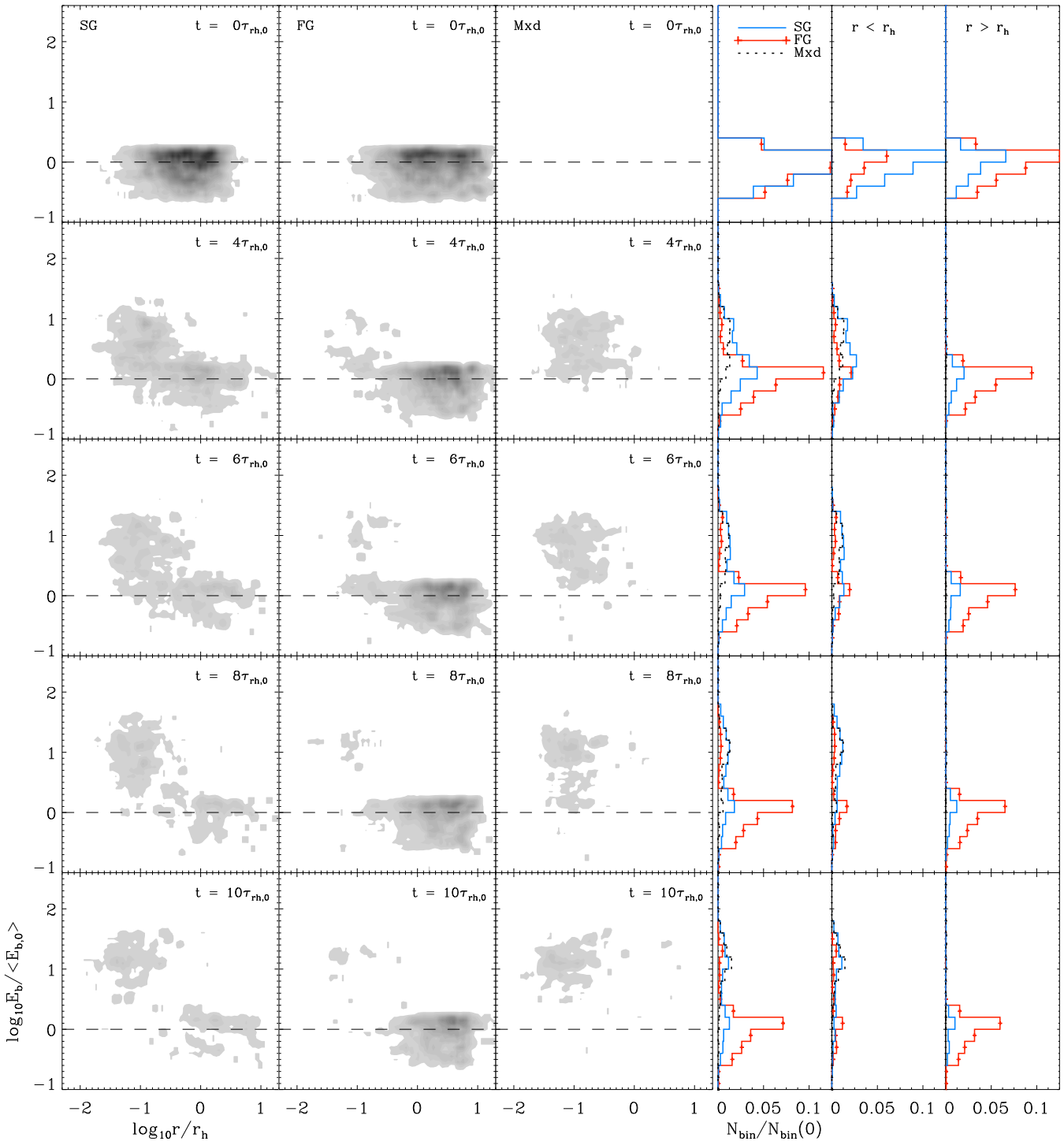

Figure 8. Time evolution of the density of SG (first column), FG (second column) and mixed (third column) binaries in the $\log(r/r_{\rm h}) - \log(E_{\rm b}/\langle E_{\rm b,0}\rangle)$ plane (where $E_{\rm b}$ is the binary binding energy and $\langle E_{\rm b,0}\rangle$ is the initial mean binding energy of all binaries for the MPr5f1x3-20 simulation). The last three columns of panels (on the right-hand side of the figure) show the histograms of the distribution of $\log(E_{\rm b}/\langle E_{\rm b,0}\rangle)$ for SG (solid blue lines), FG (red lines and short vertical segments) and mixed binaries (dashed lines) for the whole system, for binaries within the half-mass radius and outside the half-mass radius. Data from three combined snapshots around the indicated time are used for these plots.

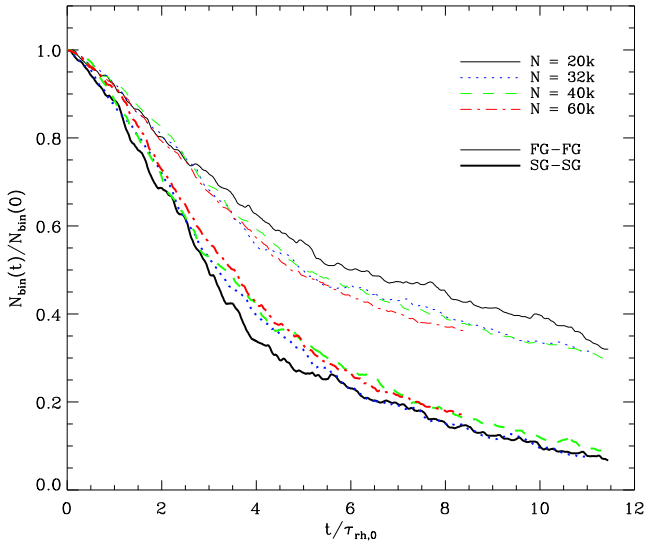

Figure 9. Time evolution of the total number of FG (thin lines) and SG (thick lines) binaries (normalized to the total initial number of binaries) for the model MPr5f03x10 and different values of the total number of particles, N (see legend in the figure). Time is normalized to the initial half-mass relaxation time.

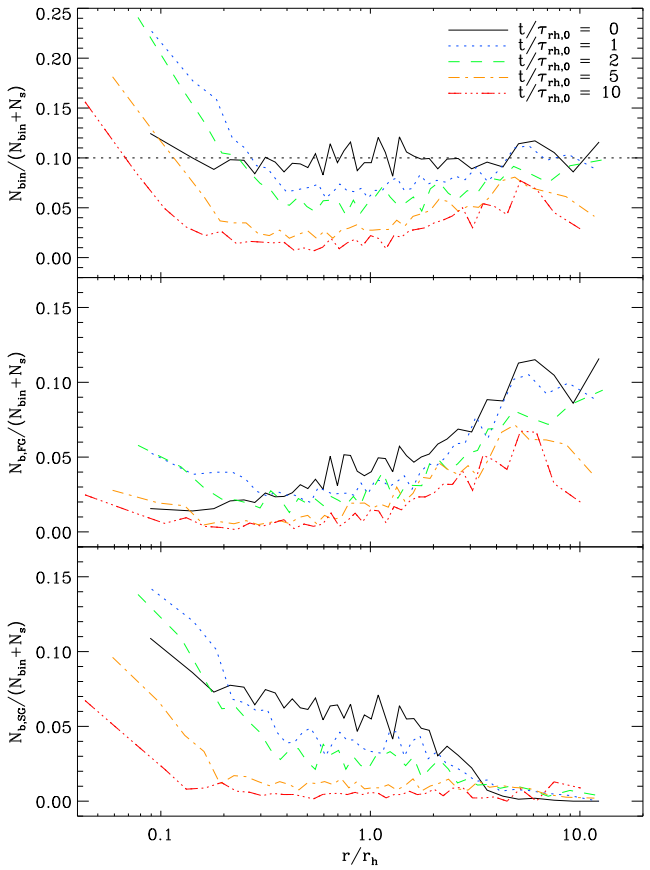

Figure 10. Time evolution of the radial profile of the binary fraction for the model MPr5f1x3-20 for all binaries (top panel), FG binaries (middle panel) and SG binaries (lower panel). Different lines in each panel correspond to the times indicated in the legend in the top panel. The radial profiles have been calculated with data from three combined snapshots around the indicated time.

(for simulations with low-binding energy binaries which are more efficiently disrupted at larger distances from the cluster centre). Observations focusing on this range of radial distances should therefore provide an approximate indication of the actual global value of the FG-to-SG binary number ratio.

4 CONCLUSIONS

In this paper we have presented the results of a survey of N-body simulations aimed at exploring the evolution of binary stars in multiple-population globular clusters. In this study we have addressed a number of fundamental aspects of the dynamics of binary stars in multiple-population clusters; in subsequent studies we will further expand this investigation by including a spectrum of masses and explore how the presence of a spectrum of masses affects the interplay among mass segregation, binary ionization, hardening and exchange interactions and the role of these processes in the dynamics of the binary population.

Theoretical models for the formation of multiple-population clusters predict that SG stars form segregated in the cluster inner regions and a number of observational studies have shown that in several clusters SG stars are more centrally concentrated and still preserve some memory of the initial segregation predicted by the formation models. The results of the simulations presented in this paper show that the initial differences between the structural properties of the SG and the FG populations may leave a fingerprint in the current properties of binary stars.

We have shown that the SG binary disruption rate is larger than that of the FG binary population. This is a consequence of the more efficient binary disruption in the cluster central high-density regions populated mainly by SG binaries. In addition to disruption, escape also affects the number of binaries in a cluster and we have shown the relative role of these processes in driving the evolution of SG and FG binaries.

The difference between the initial spatial distributions of the SG and the FG populations has also implications for the properties of the surviving binaries. Specifically, as a result of the more rapid hardening of surviving binaries in the cluster inner regions, the SG binding energy distribution is characterized by a larger fraction of binaries with large (more bound) binding energies.

We have studied the evolution of the radial variation of the SG and FG binary fraction with the distance from the cluster centre. The radial variation of the binary fraction is the result of the initial differences between the spatial distribution of the SG and FG populations and of the subsequent effects of binary segregation, disruption and escape. Although, as the cluster evolves, SG binaries are preferentially disrupted and the SG global binary fraction decreases more rapidly than that of the FG binary population, the local binary fraction in the cluster inner regions may be larger for SG binaries while the outer regions are mostly populated by FG binaries. We have shown that the SG-to-FG binary number ratio measured at a distance from the cluster centre equal to about 1–2.5r_h (where r_h is the cluster half-mass radius) is approximately equal to the global value of this ratio. Possible differences between SG and FG global and local binary fraction should be taken into account in the interpretation of observational studies aimed at exploring the properties of SG and FG binaries spanning limited range of distances from a cluster centre.

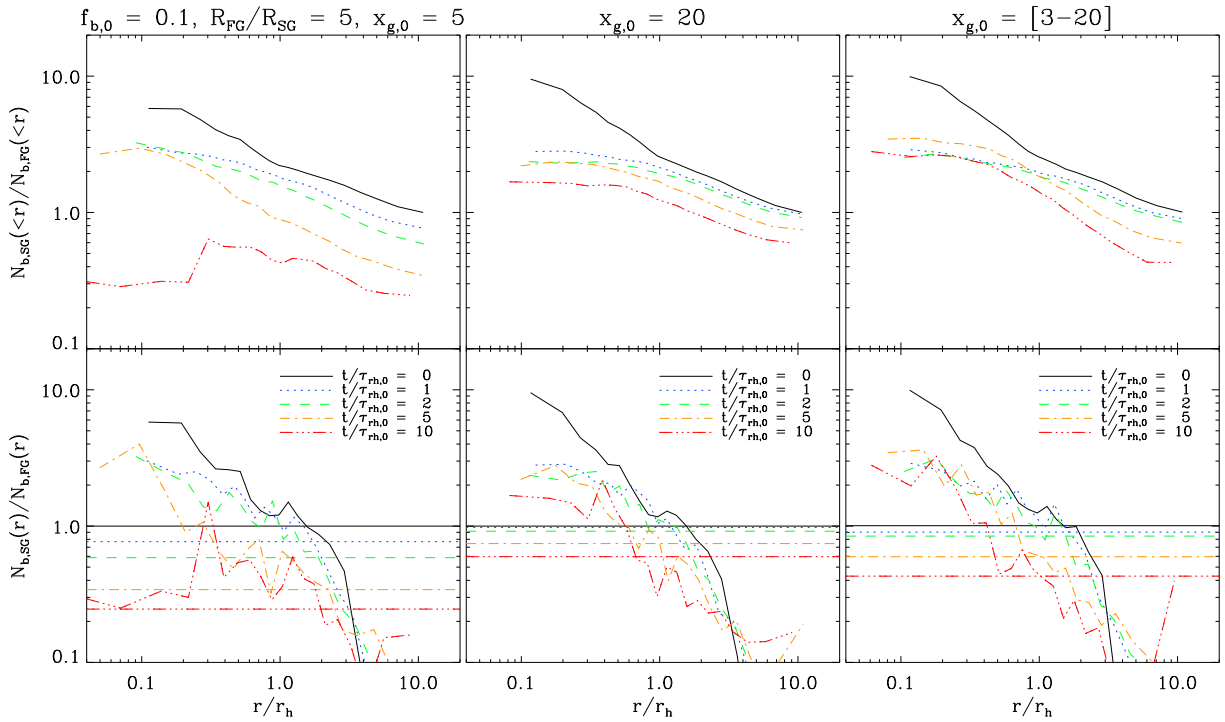

Figure 11. Top panels: time evolution of the radial profile of the ratio of the cumulative radial distributions of SG to FG binaries, $N_{\rm b,\,SG}(<r)/N_{\rm b,\,FG}(<r)$ for the simulations MPr5f1x5, MPr5f1x20 and MPr5f1x3-20. Bottom panels: time evolution of the radial profile of the SG-to-FG binary number ratio, $N_{\rm b,\,SG}(r)/N_{\rm b,\,FG}(r)$, for the simulations MPr5f1x5, MPr5f1x20 and MPr5f1x3-20; the horizontal lines indicate the global SG-to-FG binary number ratio. The radial profiles refer to the times shown in the legend in the lower panels. The radial profiles have been calculated with data from three combined snapshots around the indicated time (except for $t/\tau_{\rm rh,\,0} = 10$ for which five snapshots were used).

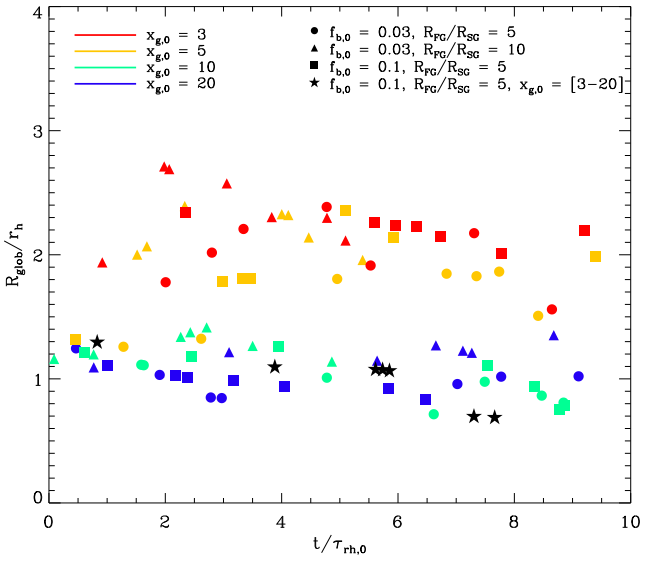

Figure 12. Time evolution of $R_{\rm glob}$, the radius where the local SG-to-FG binary number ratio equals the global value of this ratio. Different symbols and colours correspond to different simulations as indicated in the legend.

ACKNOWLEDGEMENTS

EV, JH and SLWM acknowledge support by grants NASA-NNX13AF45G and HST-12830.01-A. AS acknowledges the funding by the PRIN MIUR 2010-2011 'The Chemical and Dynamical Evolution of the Milky Way and Local Group Galaxies' (PI: F. Matteucci). This research was supported in part by Lilly Endowment, Inc., through its support for the Indiana University Pervasive Technology Institute, and in part by the Indiana METACyt Initiative. The Indiana METACyt Initiative at IU is also supported in part by Lilly Endowment, Inc.

REFERENCES

Aarseth S. J., 2003, Gravitational N-Body Simulations. Cambridge Univ. Press, Cambridge
Bastian N., Lamers H. J. G. L. M., de Mink S. E., Longmore S. N., Goodwin S. P., Gieles M., 2013, MNRAS, 436, 2398
Baumgardt H., 2001, MNRAS, 325, 1323
Beccari G., Bellazzini M., Lardo C., Bragaglia A., Carretta E., Dalessandro E., Mucciarelli A., Pancino E., 2013, MNRAS, 431, 1995
Bedin L. R., Piotto G., Anderson J., Cassisi S., King I. R., Momany Y., Carraro G., 2004, ApJ, 605, L125
Bekki K., 2011, MNRAS, 412, 2241
Bellazzini M., Bragaglia A., Carretta E., Gratton R. G., Lucatello S., Catanzaro G., Leone F., 2012, A&A, 538, A18
Bellini A., Piotto G., Bedin L. R., King I. R., Anderson J., Milone A. P., Momany Y., 2009, A&A, 507, 1393
Bellini A. et al., 2013, ApJ, 765, 32
Carretta E. et al., 2009a, A&A, 505, 117
Carretta E., Bragaglia A., Gratton R., Lucatello S., 2009b, A&A, 505, 139
Cordero M. J., Pilachowski C. A., Johnson C. I., McDonald I., Zijlstra A. A., Simmerer J., 2014, ApJ, 780, 94
D'Ercole A., Vesperini E., D'Antona F., McMillan S. L. W., Recchi S., 2008, MNRAS, 391, 825
D'Ercole A., D'Antona F., Ventura P., Vesperini E., McMillan S. L. W., 2010, MNRAS, 407, 854
D'Ercole A., D'Antona F., Carini R., Vesperini E., Ventura P., 2012, MNRAS, 423, 1521

D'Orazi V., Gratton R., Lucatello S., Carretta E., Bragaglia A., Marino A. F., 2010, ApJ, 719, L213
de Mink S. E., Pols O. R., Langer N., Izzard R. G., 2009, A&A, 507, L1
Decressin T., Meynet G., Charbonnel C., Prantzos N., Ekström S., 2007, A&A, 464, 1029
Decressin T., Baumgardt H., Kroupa P., 2008, A&A, 492, 101
Decressin T., Baumgardt H., Charbonnel C., Kroupa P., 2010, A&A, 516, A73
Ferraro F. R., Sollima A., Pancino E., Bellazzini M., Straniero O., Origlia L., Cool A. M., 2004, ApJ, 603, L81
Fukushige T., Heggie D. C., 2000, MNRAS, 318, 753
Gratton R., Carretta E., Bragaglia A., 2012, A&AR, 20, 50
Johnson C. I., Pilachowski C. A., 2012, ApJ, 754, L38
King I. R., 1966, AJ, 71, 64
Kucinskas A., Dobrovolskas V., Bonifacio P., 2014, A&A, 568, L4
Lardo C., Bellazzini M., Pancino E., Carretta E., Bragaglia A., Dalessandro E., 2011, A&A, 525, A114
Lee Y.-W., Joo J.-M., Sohn Y.-J., Rey S.-C., Lee H.-C., Walker A. R., 1999, Nature, 402, 55
Milone A. et al., 2008, ApJ, 673, 241
Milone A. et al., 2010, ApJ, 709, 1183
Milone A. et al., 2012, ApJ, 745, 58
Nitadori K., Aarseth S. J., 2012, MNRAS, 424, 545
Piotto G. et al., 2007, ApJ, 661, L53
Piotto G. et al., 2015, AJ, 149, 91
Prantzos N., Charbonnel C., 2006, A&A, 458, 135
Richer H. B., Heyl J., Anderson J., Kalirai J. S., Shara M. M., Dotter A., Fahlman G. G., Rich R., 2013, ApJ, 771, L15
Sollima A., Ferraro F. R., Bellazzini M., Origlia L., Straniero O., Pancino E., 2007, ApJ, 654, 915
Ventura P., D'Antona F., Mazzitelli I., Gratton R., 2001, ApJ, 550, L65
Vesperini E., McMillan S. L. W., D'Antona F., D'Ercole A., 2010, ApJ, 718, L112
Vesperini E., McMillan S. L. W., D'Antona F., D'Ercole A., 2011, MNRAS, 416, 355
Vesperini E., McMillan S. L. W., D'Antona F., D'Ercole A., 2013, MNRAS, 429, 1913

This paper has been typeset from a TEX/LATEX file prepared by the author.